JOURNAL OF APPLIED PHYSICS **102**, 023514 (2007)

Topography of metallic surfaces subjected to plastic strain: Roughness, spatial correlations, and eigenvalue spectral entropy

J. B. Hubbard, M. R. Stoudt,[a)] and L. E. Levine
Materials Science and Engineering Laboratory, National Institute of Standards and Technology, 100 Bureau Drive, Stop 8553, Gaithersburg, Maryland 20899-8553

(Received 12 March 2007; accepted 15 June 2007; published online 19 July 2007)

This paper describes an analysis technique that integrates high-resolution topographical imaging and rigorous matrix-based three-dimensional characterization methods. We employ scanning confocal laser microscopy to obtain topographic images of the surface of an aluminum alloy subjected to various levels of uniaxial plastic strain. These images are discretized into a square array of pixels, each of which is then assigned a numerical value corresponding to the deviation of surface height relative to an averaged background. The result is a set of real, non-Hermitian $n \times n$ matrices, which are diagonalized to produce a collection of spectra, each of which consists of n complex eigenvalues. These eigenvalue spectra are observed to change systematically as the degree of plastic strain is varied. Because this approach is based solely on the behavior of the eigenvalue spectra, it eliminates the need for the *a priori* assumptions about surface character used in conventional topographic analyses. The information contained within an eigenvalue spectrum is distilled into a scalar measure of topographic disorder, referred to as the "spectral entropy." The spectral entropy is observed to decrease monotonically with increasing plastic strain. This behavior is consistent with the observed topographical changes induced by plastic strain. In addition, the spectral entropy can be decomposed into a constant term that is independent of all spatial correlations that occur in the surface roughness and a term that incorporates these correlations at all levels of complexity.

INTRODUCTION

A plastically deformed free surface is a complex three-dimensional structure. It is, therefore, essential that such a structure be characterized in three dimensions to maximize the fidelity with the original topography. However, analysis of these highly complex topographies presents a significant challenge because many of the accepted two-dimensional approaches and analytical tools do not straightforwardly translate to a three-dimensional format.[1] This is particularly true for spatial characterizations of surface roughness.

Topographic analysis of rough surfaces incorporates aspects of geometry and multivariate statistics. The statistical aspect typically involves data condensation via a variety of projection and ensemble-averaging techniques. The principal requirement for these analyses is that the property of translationally invariant statistics (i.e., statistical stationarity or spatial homogeneity) exists. In this context, the translational invariance condition ensures that all the statistical properties, such as n-point surface height correlation functions, are invariant with respect to the location of the origin on the surface. More generally, this implies that a change in the location of a measurement does not affect the information contained within that measurement. A violation of this stationarity condition directly disputes the validity of the fundamental postulate that serves as the basis for all surface roughness analyses, namely, that a surface profile is representative of the intrinsic character of the overall surface. If this principle does not hold, then a roughness profile or any other surface statistical measure cannot reflect any inherent property of the surface from which it was taken, thereby implying that the commonly used methods to interpret surface roughness are not meaningful. It is generally recognized that the assumption of translationally invariant statistics is only approximately valid for rough surfaces, and that, in general, it must break down for systems that are too small or for correlation functions of sufficiently high order.[2] The existence of translational invariance is almost always tacitly assumed since most statistical characterizations of surface roughness utilize conventional time series analysis methods to some degree. While this assumption of statistical stationarity allows for a straightforward mathematical analysis, the literature does not provide a firm foundation to support such an ansatz. In fact, the literature clearly shows that the appropriate statistical tools must be determined by the character of the surface.[3] The statistical character of the surface can usually be determined with a classification scheme such as the one put forth by Nayak.[4]

The geometric aspect of surface roughness analysis typically involves smoothing or interpolation between neighboring measurement locations as a precursor to fitting a height profile to some analytic function. It is known that this process introduces short-range or high frequency artifacts into the mathematical expressions used to represent the original surface and depending on how the original surface is sampled, this interpolation could have a significant influence on the accuracy of the analysis.[5,6] Another geometric aspect of surface topography involves pattern recognition in a noisy environment.[7,8] For example, one might postulate the existence of a correlation between linelike surface features and grain boundaries. An appropriate filter or algorithm is then

[a)]Electronic mail: stoudt@nist.gov

applied to the image matrix in order to emphasize or enhance this type of feature. Thus, analysis techniques that minimize the significance of implicit or *ad hoc* statistical and geometrical assumptions (i.e., do not depend on the existence of stationarity, the interpolation of topographical data, or postulates about pattern recognition) are needed in order to improve the fidelity of the analysis of the measurement with respect to the original surface.

This work explores the efficacy of a representation-independent, noninterpolated measurement protocol that does not require the assumption of stationarity or the use of projected statistical quantities such as linear profiles. Furthermore, this technique does not incorporate the mathematical artifacts usually encountered in the description of finite-sized systems, such as boundary discontinuities or periodic extrapolations. The foundation of this protocol is a set of real-valued, non-Hermitian or nonsymmetric numeric matrices derived from topographic images of the surface of an aluminum alloy that is subjected to various levels of uniaxial plastic strain.[9] The images were obtained through high-resolution scanning laser confocal microscopy (SLCM). The topographies were digitized and then transformed into square arrays of numerical values that directly correspond to measured surface heights. These matrices were then diagonalized to produce a collection of spectra, each of which consisted of n complex eigenvalues, where n is the rank of the transformed image matrix. Such eigenvalue spectra are commonly employed for pattern recognition algorithms.[10]

We observed a systematic correspondence between the changes in the eigenvalue spectra and the magnitude of the plastic strain associated with the image matrix. When the spatial correlations existing in the individual image matrices were destroyed by a randomization operation, the eigenvalues migrated towards the interior of a disc centered at the origin in the complex plane. Moreover, the radius of this disc closely corresponded to the standard deviation of the surface height probability density function (σ). The standard deviation of the surface height probability density function (σ) also defines the root mean squared (rms) surface roughness (R_q), which is a universal mean roughness parameter used throughout the surface roughness literature.[11] This result is in close accord with Geman's[12] asymptotic theorem on the spectral radius of large, non-Gaussian, random matrices. Based on the high degree of conformity with this theorem, we hypothesize that certain changes in the eigenvalue spectra are due to changes in the spatial correlations within the topographies induced by the plastic strain. We will validate this hypothesis through numerical analyses and visual comparisons of the eigenvalue spectra associated with various strain states.

METALLIC SURFACE TOPOGRAPHY AND MATRICES

Aluminum alloy AA6022 in the T4 heat treatment was selected for this study because this alloy demonstrates good overall formability, it is commercially available, and the mechanical properties of this alloy in this condition are of particular interest to the automotive community. Metallographic examination revealed that the grain size ranged between approximately 10 and 90 μm. A single flat-sheet, tensile specimen was punched from 1.0 mm thick sheet stock with the tensile axis in a parallel orientation to the sheet rolling direction. The gauge section was mechanically polished to a 1 μm diamond finish using standard metallographic practice[13] and electropolished in perchloric acid to produce a strain-free surface. The tensile specimen was pulled iteratively in uniaxial tension to four nominal true plastic strain levels: 1%, 4%, 8%, and 12%. The specimen was strained at a constant crosshead displacement rate of 1.0 mm/s using a closed loop-controlled universal tensile machine. The specimen was removed from the grips for analysis after each desired strain level was achieved.

The changes in the surface morphology were quantified by examination in the SLCM. All of the SLCM images in this analysis were created with a 635 nm laser source. Typical imaging conditions consisted of a 10× objective lens and a nominal total z-scan depth of approximately 20 μm. These parameters generated a 640 pixel × 512 pixel intensity image with 12 bit resolution (i.e., 4096 sampling levels). The corresponding nominal physical dimensions (x, y, z) of these images were $1000 \times 800 \times 20\ \mu\mathrm{m}^3$. The spacing between sampling points in the x, y planes was 1.56 μm, and the spacing between the individual focal planes within each image was approximately 100 nm.

Topographic maps were generated from the intensity images with the controlling software. The SLCM stores topographic image data as a raw depth map in tagged image file format (TIFF) with each output file containing the full set of binary pixel values and the imaging parameters. A computer code that utilizes the TIFF image standards was developed to convert the individual bit values stored in the image file into a numeric matrix of surface height values. This matrix was then trimmed to a square 512 × 512 form. The height matrices were corrected for offset effects produced by specimen tilt or other mechanical influences. This "leveling" operation was performed by first computing the optimal multiple regression equation for the Euclidean plane of the image and then subtracting each point from the planar regression. The Euclidean leveling operation produced a matrix $\boldsymbol{A}$ having elements $a_{i,j}$ such that $\Sigma_{i,j} a_{i,j} = 0$. Thus, an immediate consequence of leveling is that the Euclidean or Frobenius matrix norm of this array ($\|\boldsymbol{A}\|$) is directly related to R_q by[14,15]

$$\left(\frac{1}{n}\|\boldsymbol{A}\|\right) = R_q, \tag{1a}$$

such that

$$\|\mathbf{A}\| = \left[\sum_{i,j} |a_{i,j}|^2\right]^{1/2} \tag{1b}$$

and

$$a_{i,j} \in \boldsymbol{A}, \tag{1c}$$

with

$$\sum_{i,j} a_{i,j} = 0, \tag{1d}$$

where n is the rank (e.g., 512) of the matrix $\boldsymbol{A}$. Furthermore, it follows from elementary matrix algebra that the spectral radius of the matrix $((1/n)\boldsymbol{A})$ or the magnitude (modulus) of the largest eigenvalue of that matrix, $\lambda_{\max}$, satisfies the inequality[14,15]

$$\lambda_{\max} \text{ of the matrix}\left(\frac{1}{n}\boldsymbol{A}\right) \leqslant R_q. \tag{2}$$

With the exception of trivial examples, this upper bound is weak and certainly not useful in surface analysis. However, it is also well known that if each of the elements of $\boldsymbol{A}$ are chosen independently from a single, zero-mean, or centered Gaussian distribution having the width R_q, then the following asymptotic equality holds:[16]

$$\lim_{n\to\infty} \lambda_{\max}\left(\frac{1}{\sqrt{n}}\boldsymbol{A}\right) \cong R_q. \tag{3}$$

In addition, it is known that the eigenvalues of $((1/\sqrt{n})\boldsymbol{A})$ tend to be uniformly distributed within the interior of a disc centered at the origin in the complex plane, and that the radius of this disc approaches R_q as n tends to infinity. What is not so well known is that it has been proven by Geman[12] that the asymptotic equality shown as Eq. (3) holds even for non-Gaussian distributions of matrix elements, provided that certain constraints on the higher moments of these distributions are satisfied. Given these rather abstract mathematical facts, along with certain conclusions gleaned from past and current studies of rough metallic surfaces, we infer that the concomitant patterns of eigenvalues are useful in the topographic analysis of such surfaces for the following three reasons: (1) A previous study of the height distributions of the surface of a steel alloy subjected to various intensities of strain indicated that these distributions were only approximately Gaussian.[17] As will be shown in the following section, this approximate Gaussian character also holds for the strained aluminum alloy in this study. Therefore, Geman's argument that Eq. (3) should be valid for "pseudo" as well as for "pure" Gaussian distributions has practical significance for surface roughness analysis. (2) The word "single" used in reference to the Gaussian distribution from which the elements used for Eq. (3) are selected implies statistical stationarity, so numerical conformity to these predictions can be used as a test of this important property. Therefore, it is not necessary to postulate the property of stationary statistics *a priori*. (3) Choosing elements "independently" from a single Gaussian distribution ensures the absence of any spatial correlations. Thus, analyzing the deviations from the prediction of Eq. (3) in conjunction with the deviations of the entire eigenvalue spectrum from a uniform distribution enclosed by a disc of radius R_q establishes a tool for probing surface height correlations of arbitrary complexity. That is, it is not necessary to restrict the analysis to correlations of low order, such as those at the two or three point level. Stated more generally, these eigenvalue spectra serve as minimally biased "fingerprints" that are independent of implicit or *ad hoc* statistical or geometric assumptions, as well as being independent of any particular mathematical form, i.e., eigenvector representation, chosen to characterize the surface topography.

MOMENTS OF THE HEIGHT DISTRIBUTION AND SURFACE AREA

Figure 1 shows the topographies of the aluminum alloy at the four levels of uniaxial plastic strain. The lighter regions correspond to elevations relative to the average level plane, while the darker features correspond to depressions. Note that the height correlations tend to be more prominent at the higher strain levels. Surface height probability density profiles for the four levels of strain are presented in Fig. 2. Note that the height distributions are approximately Gaussian in shape, and that they exhibit a pronounced broadening with increasing strain.

The first four statistical moments of the height distributions are given in Table I. The values shown were calculated directly from the normalized frequency histograms consisting of all 262 144 elements in the image matrix; i.e., every element of $\boldsymbol{A}$ is sampled and included in each calculation. As expected, the surface means are effectively zero; hence, a matrix norm algorithm based on Eq. (1) can be used to calculate the standard deviation (i.e., R_q). Note that R_q grows monotonically with increasing strain, and that the third moments are small and negative so that, in general, valleys of a given depth are slightly more probable than peaks of that same height. In accordance with a previous study,[17] the normalized fourth moments are quite a bit larger than the Gaussian value of 3 for low strain levels and narrow probability distributions, which implies that under these conditions surface roughness is composed of artifacts introduced by the polishing and etching operations. However, these moments appear to approach the Gaussian value at the highest strains. For this reason, we hypothesize that this approximate conformity to the central limit theorem of statistics reflects the emergence of multiple independent deformation components (e.g., primary slip, secondary slip, grain rotation, etc.) at high strain levels.[17]

The estimated surface area values, relative to a perfectly flat plane, were computed via a pixel-based code that tessellates the surface with triangles, each having various orientations with respect to the planar normal.[18] While the surface areas shown in Table I are resolution-dependent quantities, they do not vary at low strains and they increase moderately at high strain.

EIGENVALUE SPECTRA AND SPATIAL CORRELATIONS

As a concrete illustration of the general method outlined in the previous section, Fig. 3 shows all 512 "normalized" complex eigenvalues of the image matrix $\boldsymbol{A}$, i.e., $(\lambda((1/\sqrt{n})\boldsymbol{A}))$ for the four degrees of uniaxial plastic strain. A careful inspection of the numeric data indicates the following: (a) no two eigenvalues are identical; (b) no eigenvalue is purely imaginary or zero; and (c) the largest eigenvalues tend to be real. Note that the eigenvalues appear in complex conjugate pairs, and that there is a clear correlation between strain intensity and the location of the largest eigenvalues. Furthermore, as shown in Table II, the magnitude of the largest eigenvalue $\lambda_{\max}$ (i.e., the spectral radius) always exceeds the standard deviation of the height distribution, σ (column

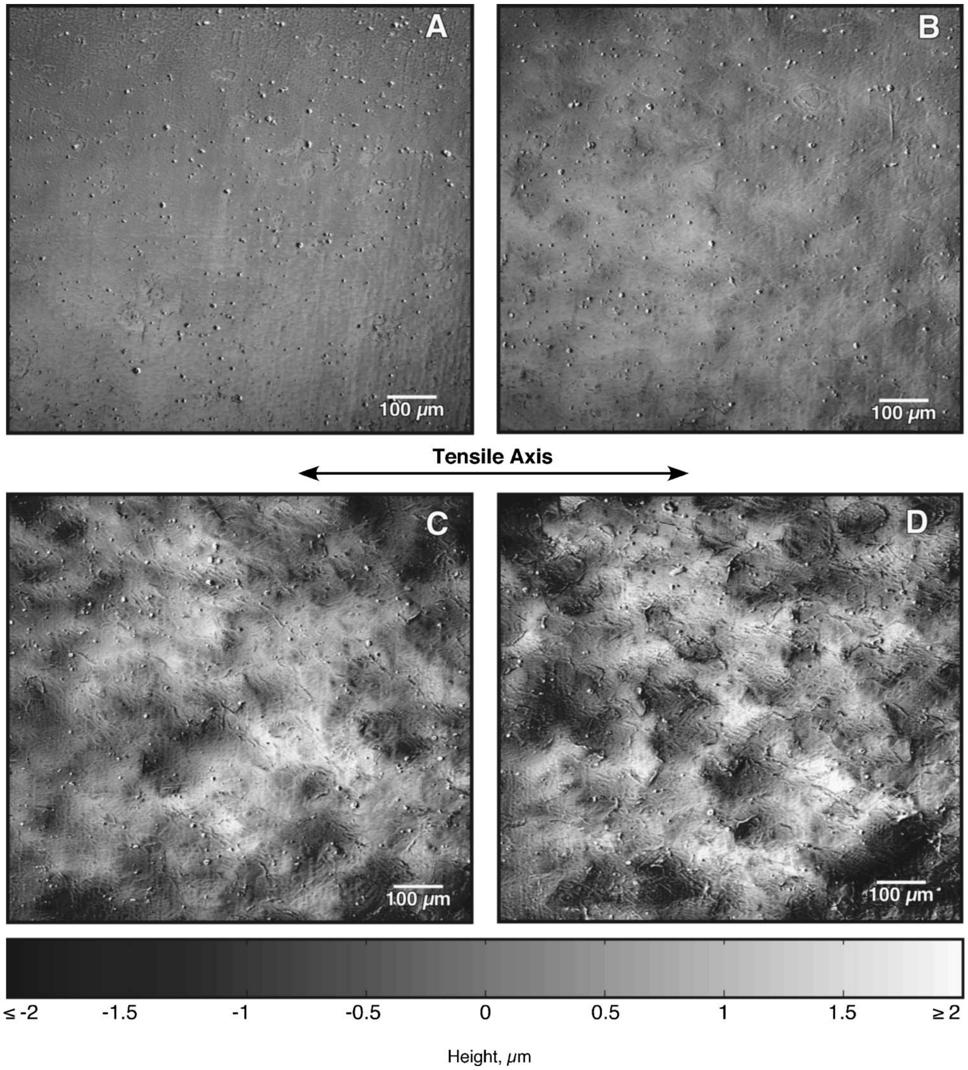

FIG. 1. The topographies of the deformed surfaces of AA6022 produced by uniaxial tension. These images were acquired with scanning laser confocal microscopy. (a) With 1% plastic strain, (b) with 4% plastic strain, (c) with 8% plastic strain, and (d) with 12% plastic strain.

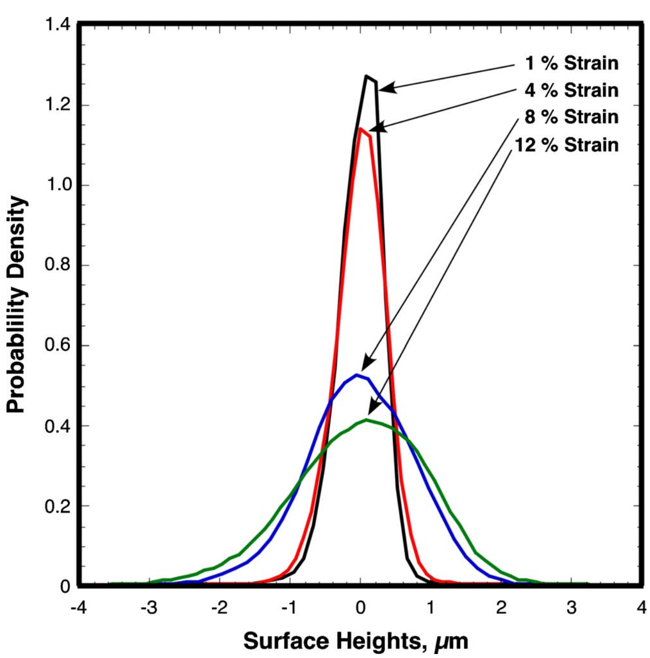

FIG. 2. (Color online) The normalized surface roughness probability histograms for the four strain intensities shown in Fig. 1.

five in Table I). Therefore, the relationship shown in Eq. (3) is not satisfied. It can be demonstrated that the spatial correlations between elements within the image matrix are responsible for this discrepancy by implementing a code that divides $\boldsymbol{A}$ into submatrices of size $2^m \times 2^m$ (where m ranges from 3 to 9). This code then randomly permutes, or scrambles, all of the elements contained within each submatrix. The effects of progressive scrambling on the spectra for the 1% and 12% strain states are presented in Figs. 4 and 5 and in Table III. The solid oval lines in Figs. 4 and 5 are the boundaries that separate eigenvalues whose moduli are less than R_q from those eigenvalues whose moduli are greater than R_q. In these figures, $\lambda_{\max}$ exceeds R_q up to the value of $m=7$. This implies the existence of long range, albeit weak, spatial correlations. However, scrambling the entire image matrix (i.e., $m=9$) brings $\lambda_{\max}$ into near identity with R_q, in accordance with Eq. (3). A comparison between Tables II and IV indicates that the standard deviations in the eigenvalue moduli are drastically reduced by randomizing the elements of $\boldsymbol{A}$. This compaction of the distribution is due primarily to the reduction of the moduli of the largest eigenvalues.

The eigenvalue moduli can also be presented in an alternative manner. Figures 6 and 7 are log plots showing the moduli associated with the fully randomized and the corre-

TABLE I. Statistical properties of height distributions derived from correlated topographies.

Strain level (%)	Surface area (μm^2)	Mean σ_1 (μm)	Variance σ_2 (μm^2)	Std. dev. σ (μm)	Skew σ_3 (μm^3)	Kurtosis σ_4 (μm^4)
1	$6.593E+05$	$4.61E-10$	0.1588	0.3985	−0.9030	27.9526
4	$6.572E+05$	$-3.99E-09$	0.1807	0.4251	−0.6235	14.0182
8	$6.865E+05$	$-2.61E-08$	0.6510	0.8068	−0.1385	5.6557
12	$7.115E+05$	$1.66E-08$	0.9489	0.9741	−0.2750	3.4438

lated image matrices plotted against the eigenvalue number (1-512). Note that in each figure, the largest magnitude corresponds to the first eigenvalue (1). There are two principal advantages of representing the eigenvalues in this fashion: First, the plot of the randomized image matrix eigenvalues (Fig. 7) eliminates any influence of spatial correlations from the overall behavior of the distribution. This enables direct assessments of how an increase in plastic strain affects the overall eigenvalue distributions for the four individual strain states. While the overall shapes of the distributions shown in Fig. 6 are quite similar, the height or magnitude of a distribution increases with plastic strain. As expected, this behavior is consistent with the changes observed in the range of probable heights shown in Fig. 2. The second advantage of the log plot is clearly exhibited in Fig. 7. As shown, the overall shapes of the four distributions are largely similar to those shown in Fig. 6 for the larger eigenvalue indices. However, the spatial correlations present in these data sets induced pronounced deviations at the low eigenvalue numbers (i.e., from eigenvalues 1 through approximately 30). The magnitudes of these deviations appear to scale proportionally with plastic strain.

Because we have isolated the effect of an increase in plastic strain (Fig. 6) on the eigenvalue distribution from the changes in correlation produced by the increase (Fig. 7), we are able to examine the influence of plastic strain on the eigenvalue distribution. In addition, the first eigenvalues shown in Fig. 6 now closely match R_q, in accordance with the prediction of Eq. (3); the implications of this congruence will be considered in the following section.

SPECTRAL MOMENTS AND SPECTRAL ENTROPY

We now compare low-order statistical moments of the full non-Hermitian spectra of the image matrices with those of their Hermitian projections for each strain level, as shown in Tables II and V. We also list the two largest eigenvalues, which happen to be real, for the four strains. Note that the full spectral mean or average is, in each case, close to zero, whereas the average eigenvalue magnitude increases monotonically with strain. This behavior reflects the near-exact symmetry of the eigenvalue pattern with respect to reflection through the origin, in contrast with the positive-definite asymmetry of its Hermitian projection. However, the stan-

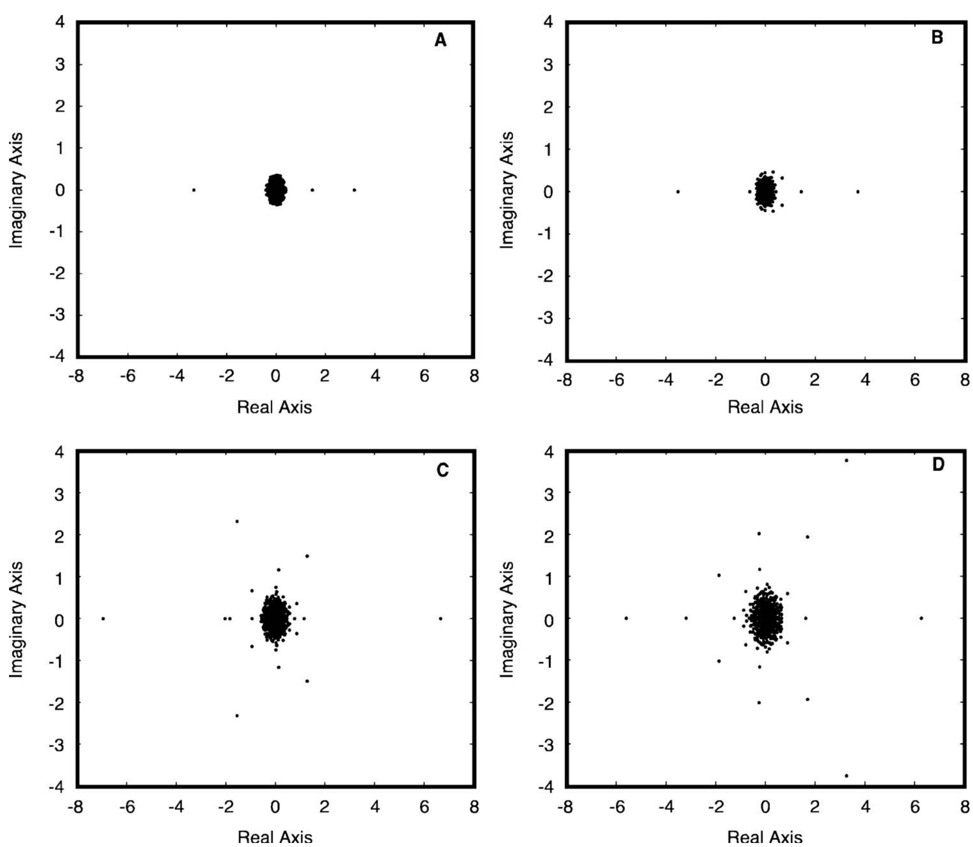

FIG. 3. (Color online) Plots of the locations of all 512 complex eigenvalues associated with the fully correlated image matrices for 1% strain in A, 4% strain in B, 8% strain in C, and 12% strain in D.

TABLE II. Statistical properties of eigenvalue moduli derived from correlated topographies.

Strain level (%)	λ_{max} (μm)	2nd largest λ (μm)	Mean λ (μm)	Std. deviation σ_λ (μm)
1	3.3221	3.1696	0.2634	0.2247
4	3.7089	3.5150	0.2821	0.2504
8	6.9435	6.6674	0.5364	0.4972
12	6.2790	5.6008	0.6458	0.5631

dard deviations of the complex spectra correlate rather well with those of the corresponding moduli. As might be expected, the higher moments, which are not listed, vary markedly from one another and they correlate poorly with the degree of strain.

As seen in Figs. 3–5, the eigenvalue spectra can be characterized as compact, disc-shaped clouds of points centered at the origin in the complex plane; these discs are surrounded by sparsely distributed halos of eigenvalues having relatively large moduli. This description can be made quantitative by disregarding the phases and focusing on the total number of eigenvalues residing within the discs of continually increasing radii. As shown in Fig. 8, the behavior of the number of enclosed eigenvalues is sensitive to whether the elements in the image matrix are correlated or fully randomized. For the randomized case, the number enclosed for the smallest 500 eigenvalues closely follows a parabolic r^2 profile, which indicates a uniform distribution. This observation is in excellent conformity with certain mathematical theorems on large random matrices.[12] In contrast, the number of enclosed eigenvalues associated with the correlated image matrix has a profile varying approximately as $r^{1/2}$. The key point is that the entire eigenvalue spectrum, and not just the satellite eigenvalues, is quite sensitive to the presence of any spatial correlations within the image matrix.

Motivated by concepts usually associated with information theory,[19–23] we construct a discrete probability measure that is based on the eigenvalue moduli. By considering an ensemble of $n \times n$ image matrices along with their associated eigenvalue spectra $\{\lambda_1, \lambda_2, \ldots, \lambda_n\}$, we can define the probability $p(|\lambda_i|)$ for the "occurrence" of the ith magnitude as

$$p(|\lambda_i|) = \left[\frac{|\lambda_i|}{\sum_{i=i}^{n} |\lambda_i|} \right], \tag{4}$$

where $n=512$, and thereby ensure the normalization,

$$\sum_{i=1}^{n} p(|\lambda_i|) = 1 . \tag{5}$$

We now use this set of probabilities to define "spectral entropy" (SE) as

$$\mathrm{SE} = -\left[\sum_{i=1}^{n} p(|\lambda_i|) \ln p(|\lambda_i|) \right], \tag{6}$$

where $\mathrm{SE} \geqslant 0$. A plot of SE versus strain is shown Fig. 9. For the correlated image matrices, SE decreases monotonically with strain, whereas it is virtually independent of strain for the fully randomized matrices. This invariance is remarkable in consideration of the fact that, as shown in Fig 2, surface height probability densities vary markedly with plastic strain.

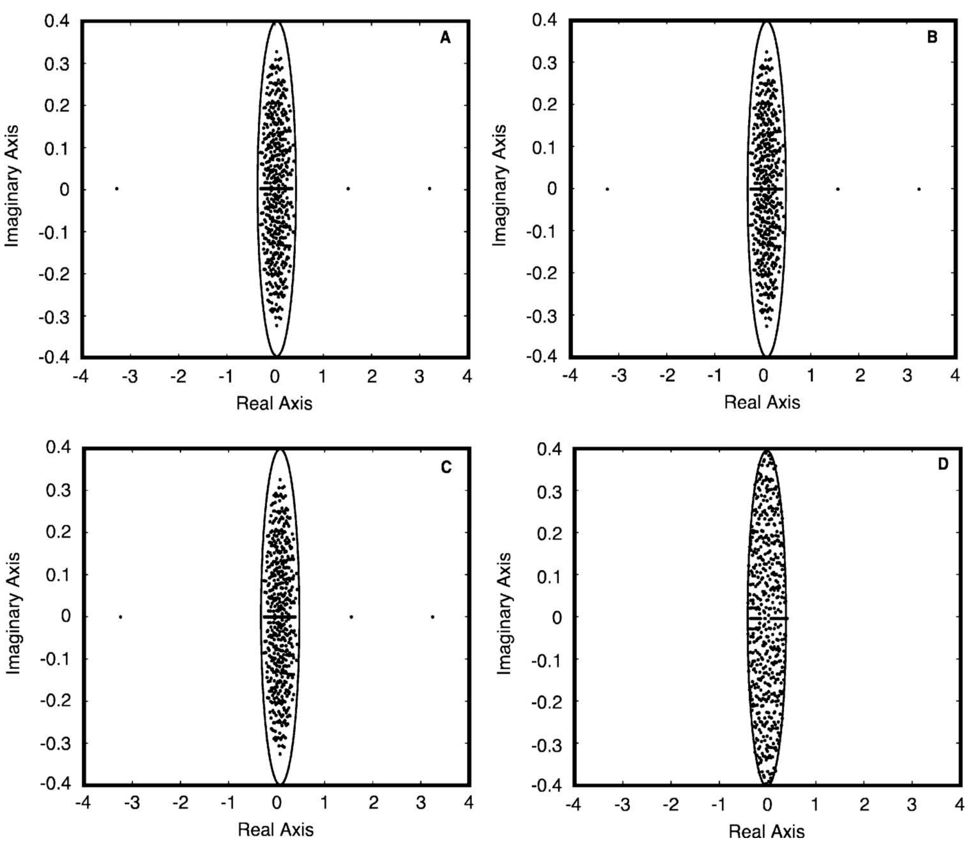

FIG. 4. Plots of the locations of all 512 complex eigenvalues associated with the progressively randomized image matrices for the 1% plastic strain level. Note that each figure exhibits a random permutation of all matrix elements with blocks of 2^m where m is equal to 3 in A, 4 in B, 7 in C, and 9 in D.

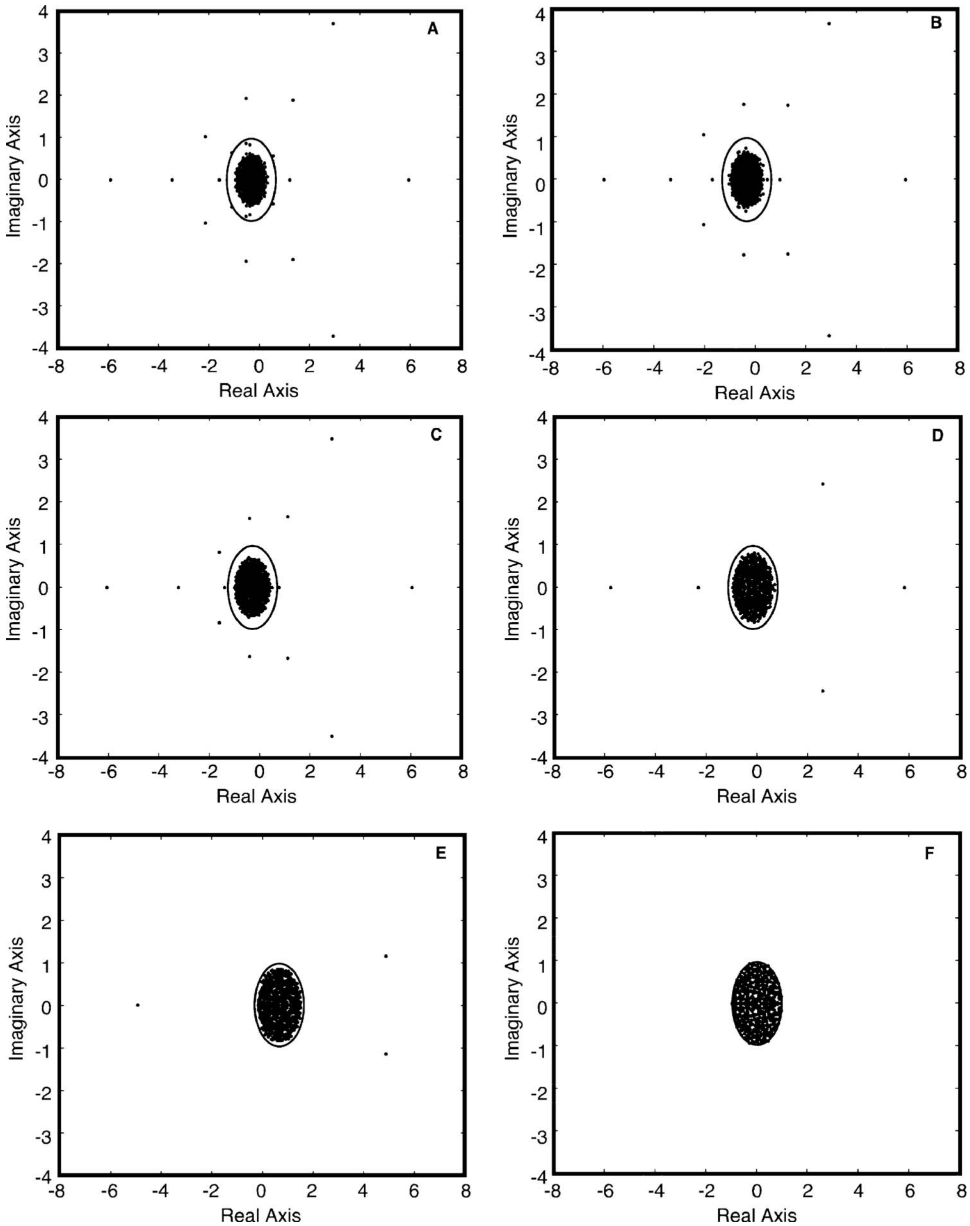

FIG. 5. Plots of the locations of all 512 complex eigenvalues associated with the progressively randomized image matrices for the 12% plastic strain level. Note that each figure exhibits a random permutation of all matrix elements with blocks of 2^m where m is equal to 3 in A, 4 in B, 5 in C, 6 in D, 7 in E, and 9 in F.

The decrease in the entropy with increasing strain exhibited in Fig. 9 indicates a decrease in the effective number of topographic degrees of freedom. That is, the surface topography tends to become more ordered or correlated with strain. It should also be noted that the constant spectral entropy associated with the randomized topographies is not a maximum. The "ideal" or maximally random value shown as the line in Fig. 9 is given by $\ln(512)=6.2383$. This corresponds to eigenvalues distributed on the circumference of a circle centered at the origin in the complex λ plane. Given our definition of SE [Eq. (6)], these maximally disordered spectra are then associated with the class of "unitary" topographic image matrices.[14,15,24] In a future publication, we will show how the implementation of a computational algorithm for the "relative spectral entropy"[25] or the "Kullback-Leibler divergence"[26,27] can be used to quantify differences among the eigenvalue spectra associated with a set of topographic images.

TABLE III. The influence of progressive scrambling on the eigenvalue behavior.

Strain level (%)	Scramble index m	Incremental surface area (μm^2)	λ_{max} (μm)
1	0	6.593E+05	3.3221
1	3	6.749E+05	3.3199
1	4	6.765E+05	3.3112
1	5	6.779E+05	3.2926
1	6	6.803E+05	3.2129
1	7	6.874E+05	2.8830
1	9	7.033E+05	0.4215
12	0	7.115E+05	6.2790
12	3	7.747E+05	6.2538
12	4	7.966E+05	6.2659
12	5	8.300E+05	6.3306
12	6	8.760E+05	5.9674
12	7	9.187E+05	5.5879
12	9	9.711E+05	0.9879

TABLE IV. Statistical properties of eigenvalue moduli derived from randomized topographies.

Strain level (%)	λ_{max} (μm)	2nd largest λ (μm)	Mean λ (μm)	Std. deviation σ_λ (μm)
1	0.4215	0.4055	0.2634	0.0943
4	0.4392	0.4347	0.2821	0.1010
8	0.8152	0.8003	0.5364	0.1916
12	0.9879	0.9802	0.6458	0.2300

TABLE V. Statistical properties of complex eigenvalues derived from correlated topographies

Strain level (%)	λ_{max} (μm)	2nd largest λ (μm)	Mean λ (μm)	Std. deviation σ_λ (μm)
1	−3.3221	3.1696	−0.0009	0.2800
4	3.7089	−3.5150	−0.0009	0.2999
8	−6.9435	6.6674	−0.0007	0.5701
12	6.2790	−5.6008	−0.0020	0.6861

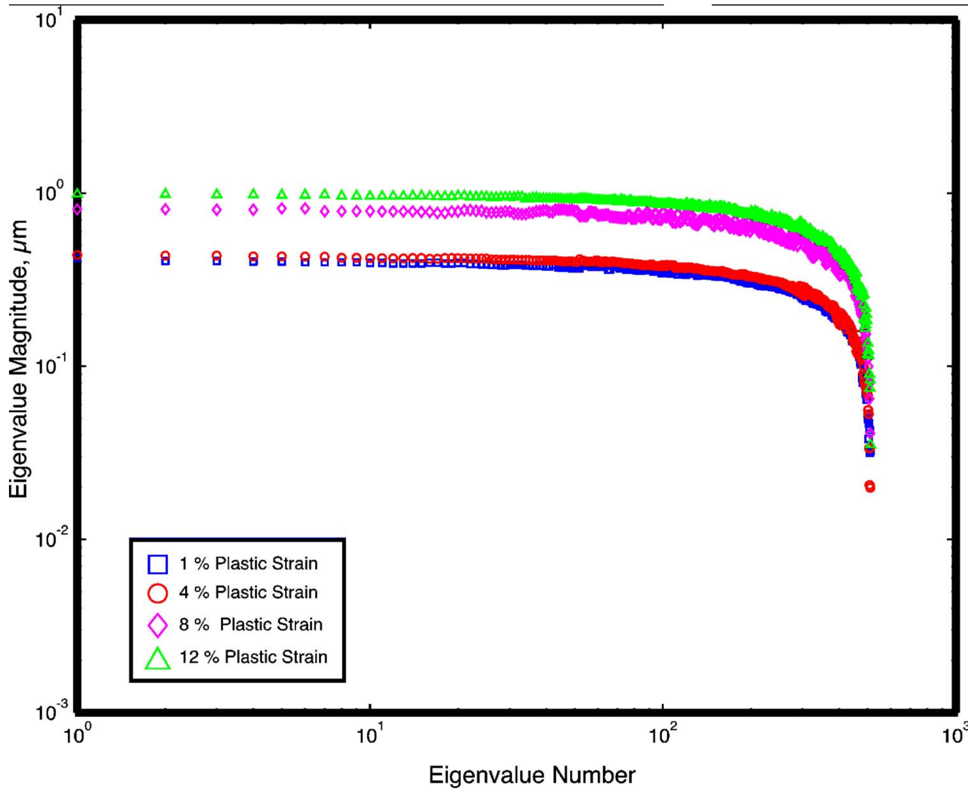

FIG. 6. (Color online) Log plot of the eigenvalue modulus vs the ordered eigenvalue number associated with the fully randomized image matrices for the four plastic strain intensities.

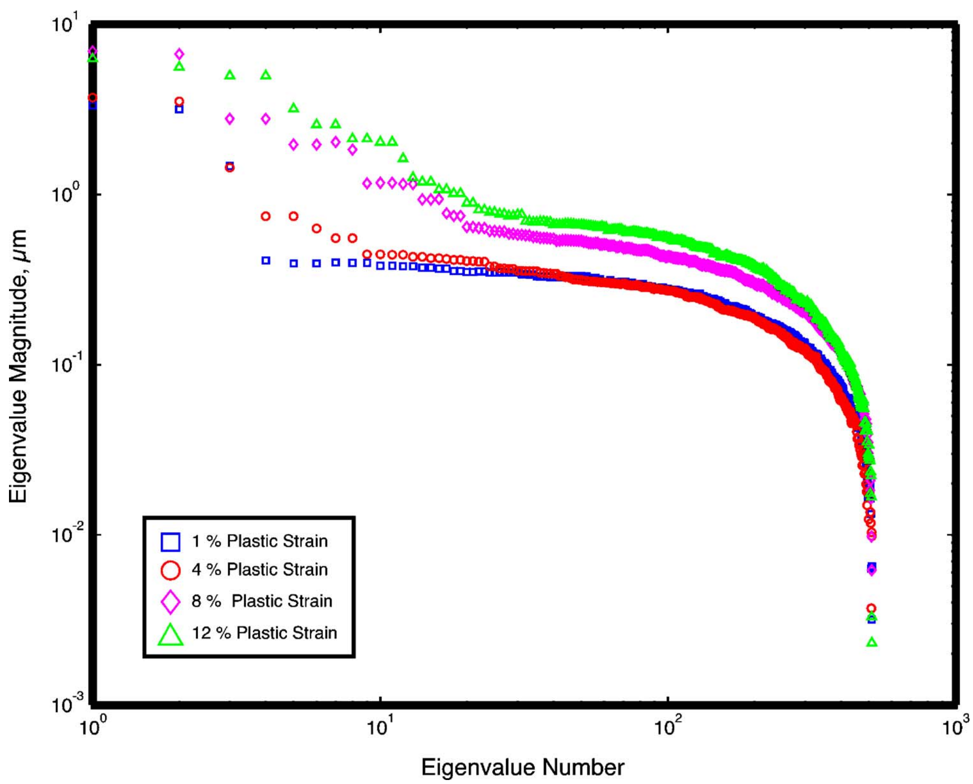

FIG. 7. (Color online) Log plot of the eigenvalue modulus vs the ordered eigenvalue number associated with the fully correlated image matrices for the four plastic strain intensities.

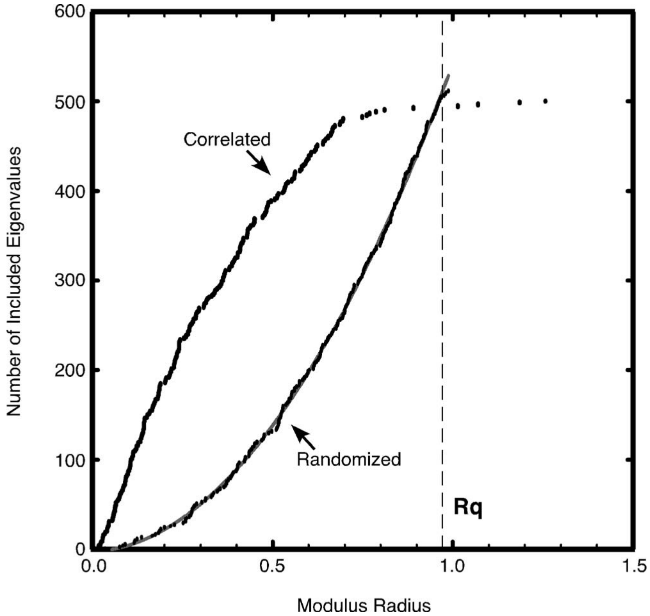

FIG. 8. The total number of eigenvalues enclosed within discs of various radii for the 12% strain topography. Each disc is centered at the origin of the complex plane.

DISCUSSION

A central issue in our analysis is the convergence or stability of the normalized eigenvalue distributions as n becomes large. We have dissected our 512×512 matrices into sets of smaller square matrices down to the 8×8 level to address this point. Although the eigenvalue spectra for the smaller matrices are quite variable from one another, we begin to observe a pronounced regularity at $n=128$. This is approximately the size at which our block randomization algorithm begins to generate uniform eigenvalue patterns. These patterns are contained within a disc that has a radius that is equal to R_q. While we cannot rule out the asymptotic notion that Geman's spectral radius theorem should hold for any "pseudo-Gaussian" random matrix of sufficiently large rank with "short range correlations" between individual elements, we conclude that n must be considerably larger than 512 for this to occur. Not surprisingly, this implies that the eigenvalue spectra of our image matrices must depend on the degree of spatial resolution. In any case, this conundrum illustrates the intrinsic ambiguity associated with any comparison between the statistical properties of finite-size disordered systems and the convergence to asymptotic limits.

The surface topography eigenvalue spectra are characterized by a relatively compact, disc-shaped core centered at the origin in the complex plane; this core is enveloped by a sparse halo of satellite eigenvalues, and the eigenvalue with the largest magnitude (the spectral radius) tends to lie on the real axis. The destruction of spatial correlations in the surface roughness at the two-points and all higher order levels is achieved by block randomization of the locations of all matrix elements in $2^m\times2^m$ blocks, with m varying from 3 to 9. This set of transformations results in the migration of the satellite eigenvalues towards the origin, along with a tendency for the smaller eigenvalues to increase their magnitudes to uniformly fill a disc of radius R_q.

It must be emphasized that, in general, no relationship, either observed or postulated, between surface topography and plastic strain can be regarded as unique. This is a result of both surface structure and bulk plastic deformation being path dependent rather than state-dependent parameters. In the case of uniaxial strain, the deformation trajectory is linear, which implies that some, though not all, ambiguity has been removed. A measurement and description of topography in terms of a state-dependent tensor quantity such as local surface stress is beyond the scope of this particular investigation.

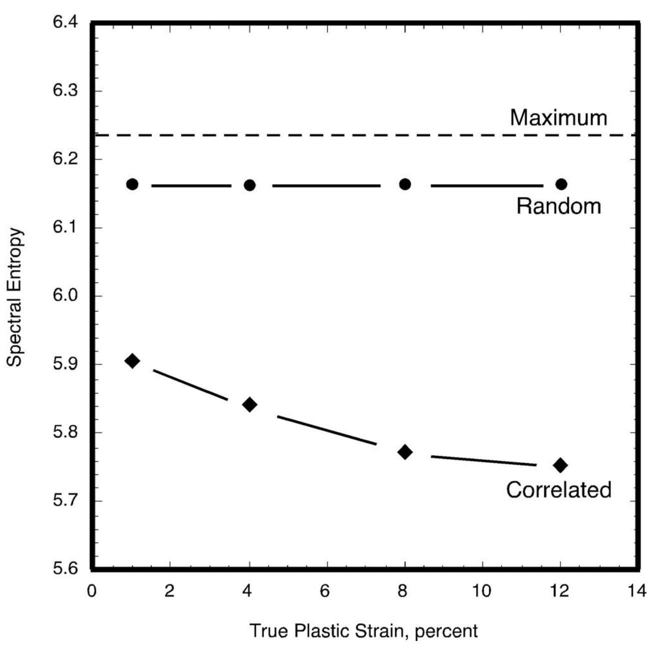

FIG. 9. A plot of the $\Sigma p\ \ln(p)$ spectral entropy vs plastic strain for the four strain conditions. The entropy associated with the randomized topographies is insensitive to strain whereas the entropy associated with the correlated topographies decreases monotonically with strain. The maximum spectral entropy is given by ln(512) or 6.2383.

CONCLUSIONS

This paper presents an eigenvalue-based analysis of roughened metallic surfaces that possesses the following advantages over conventional approaches: (1) The assumption of translationally invariant statistics is not required. (2) Interpolation or smoothing of the raw data is avoided. (3) The original three-dimensional surface is not represented by projections of two-dimensional profiles. (4) Each element of the analysis is based on the entire image data set. (5) This technique does not introduce mathematical artifacts such as boundary discontinuities or periodic extrapolations. Although this eigenvalue-based approach requires mathematical abstractions that differ from what are employed in conventional topographic analysis, these advantages justify its use to assess changes in the spatial correlations that occur as a function of the plastic deformation.

The information contained within an eigenvalue spectrum is distilled into a scalar measure of topographic disorder, referred to as the "spectral entropy" (SE). This entropy, whose form is virtually identical to that encountered in information theory and statistical physics, is observed to decrease monotonically with increasing plastic strain. This behavior appears to be consistent with the observed topographical changes induced by plastic strain. Moreover, the SE can be decomposed into a constant term that is independent of all spatial correlations that occur in surface roughness and a term that incorporates these correlations at all levels of complexity.

It should be emphasized that this is a preliminary study. We do not attempt to address issues such as the possible connections between eigenvalue spectra, eigenvalue migration trajectories, and various surface roughening mechanisms. Additional studies to address these issues are in development.

[1] *Three Dimensional Surface Topography; Measurement, Interpretation and Applications*, edited by K. J. Stout (Penton, London, 1994).
[2] N. G. vanKampen, *Stochastic Processes in Physics and Chemistry* (North-Holland, Amsterdam, 1981).
[3] M. S. Longuet-Higgins, Philos. Trans. R. Soc. London, Ser. A **250**, 157 (1957).
[4] P. R. Nayak, ASME J. Lubr. Technol. **93**, 398 (1971).
[5] J. A. Greenwood, Proc. R. Soc. London, Ser. A **393**, 133 (1984).
[6] W. P. Dong, E. Mainsah, and K. J. Stout, Int. J. Mach. Tools Manuf. **36**, 1347 (1996).
[7] J. Serra, *Image Analysis and Mathematical Morphology* (Academic, London, 1982).
[8] G. Winkler, *Image Analysis, Random Fields and Markov Chain Monte Carlo Methods: A Mathematical Introduction*, 2nd ed. (Springer, Berlin, 2000).
[9] M. R. Stoudt, J. B. Hubbard, S. A. Janet, and J. Liu, in *Sixth Global Innovations Symposia on Materials Processing: Trends in Materials and Manufacturing Technologies and Powder Metallurgy R&D in the Transportation Industries*, edited by T. R. Bieler, J. E. Carsley, H. L. Fraser, and J. E. Smugeresky (TMS, Warrendale, PA, 2005), pp. 89–94.
[10] M. Turk and A. Pentland, J. Cogn Neurosci. **3**, 71 (1991).
[11] Anonymous, *ASME Designation B46.1-2002: Surface Texture (Surface Roughness, Waviness and Lay)* (American Society of Mechanical Engineers, New York, NY, 2002).
[12] S. Geman, Ann. Probab. **14**, 1318 (1986).
[13] G. F. VanderVoort, *Metallography Principles and Practice* (ASM International, Materials Park, OH, 1999).
[14] R. Bellman, *Introduction to Matrix Analysis*, 2nd ed. (McGraw-Hill, New York, 1976).
[15] P. Lancaster and M. Tismenetsky, *The Theory of Matrices* (Academic, New York, NY, 1985).
[16] J. Ginibre, J. Math. Phys. **6**, 440 (1965).
[17] M. R. Stoudt and J. B. Hubbard, Acta Mater. **53**, 4293 (2005).
[18] M. Cai, M. R. Stoudt, L. E. Levine, and J. T. Dickinson, Philos. Mag. **87**, 907 (2007).
[19] http://en.wikipedia.org/wiki/Information_theory
[20] R. B. Ash, *Information Theory* (Dover, New York, 1990).
[21] M. R. Fazlollah, *An Introduction to Information Theory* (Dover, New York, 1994).
[22] A. I. Khinchin, *Mathematical Foundations of Information Theory* (Dover, New York, 1957).
[23] C. E. Shannon and W. Weaver, *The Mathematical Theory of Communication* (University of Illinois Press, Urbana, 1949).
[24] R. Bronson, *Matrix Operations* (McGraw-Hill, New York, NY, 1989).
[25] http://en.wikipedia.org/wiki/Quantum_relative_entropy
[26] http://en.wikipedia.org/wiki/Kullback%E2%80%93Leibler_divergence
[27] S. Kullback and R. A. Liebler, Ann. Math. Stat. **22**, 79 (1951).